PCCP

ROYAL SOCIETY OF CHEMISTRY

PAPER

View Article Online
View Journal | View Issue

Cite this: *Phys. Chem. Chem. Phys.*, 2024, **26**, 17882

Co-doped $NaYF_4$:Yb/Er/Tm upconversion luminescent coating to enhance the efficiency of photovoltaic cells†

Shaoqi Zhu,[ab] Xiaofeng Xie, *[ab] Lin Han,[c] Haiming Li,[c] Chenglin Shi,[c] Yong Yang[c] and Jing Sun *[ab]

Received 31st January 2024,
Accepted 5th June 2024

DOI: 10.1039/d4cp00459k

rsc.li/pccp

The use of upconversion luminescent materials to broaden the utilization range of the solar spectrum to enhance the efficiency of photovoltaic cells offers a promising and sustainable approach. However, the low luminescence intensity and easy quenching of upconversion luminescent materials bring serious challenges to the practical application. Herein, a novel method using Co^{2+} ion doping to regulate the luminescence properties of $NaYF_4$:Yb/Er/Tm is proposed. $NaYF_4$:Yb/Er/Tm microcrystals doped with different proportions of Co^{2+} ions are prepared and used as coatings on the surface of photovoltaic cells. Co^{2+} ions regulate the crystallinity and size of the $NaYF_4$:Yb/Er/Tm microcrystals and reduce the crystal field symmetry of the activator (Er^{3+} and Tm^{3+}) ions. The results show that the emission intensity of green and red light is 18.19% and 83.24% times higher than that of undoped Co^{2+} ion materials, respectively. Besides, the efficiency of photovoltaic cells after coating Co^{2+} ion doped $NaYF_4$:Yb/Er/Tm is 2.08% higher than that of the uncoated one. This work underscores the importance of Co^{2+} ion doping to improve and enhance the luminescence properties of $NaYF_4$:Yb/Er/Tm, to further enhance the efficiency of photovoltaic cells.

1. Introduction

The development of photonic conversion materials could harness an underutilized part of the solar spectrum to address the growing demand for renewable energy.[1] Photovoltaic cells absorb solar radiation in the wavelength range of 300–1100 nm, mainly absorbing visible photons, while infrared photons are not fully utilized.[2,3] A wider absorption spectrum is very much needed in photovoltaic cell applications.[4] The current annual use of solar energy is well below 1% of the total energy consumption, and more efficient and cheaper photovoltaic systems must be developed to achieve large-scale energy utilization.[5] In the past decade, there have been many research studies related to upconversion phenomena, including the luminescence mechanism, material design and application.[6–9] Rare-earth doped upconversion luminescent materials can convert infrared photons to visible photons by upconversion luminescence and so broaden the spectral response range of photovoltaic cells to solar irradiation and improve the light absorption capacity and photoelectric conversion efficiency of photovoltaic cells.[10] β-$NaYF_4$ is considered one of the most efficient host materials for upconversion luminescence with combining a Yb^{3+} sensitizer and an activator (Er^{3+}, Tm^{3+}, and Ho^{3+}) under infrared excitation.[11] Many lanthanide (Ln)-doped upconversion luminescence materials have been successfully synthesized based on solvothermal, hydrothermal, precipitation and thermal decomposition methods.[12,13] However, the upconversion luminescent materials doped with rare earth elements have the problems of low fluorescence intensity and easy quenching, which limits the application in improving the photovoltaic performance.[14] Based on the research over the past decade, Goldschmidt *et al.*[4] concluded that the upconversion field needs further development to become a relevant technology choice in the photovoltaic field.

Previously, intensive efforts have been put to improve the upconversion luminescence intensity of $NaYF_4$:Ln^{3+}, such as *via* core–shell structure construction,[15] plasmon resonance,[16,17] dye sensitization, ion exchange and so on.[18] But the synthesis of high-quality $NaYF_4$:Ln^{3+} with specific sizes and morphologies in a simple way is still a challenge.[19] Impurity doping has recently been recognized as having a significant influence on the crystal phase, size and luminescence properties of $NaYF_4$:Ln^{3+} materials with simple synthesis.[20,21] The results show that transition metal

[a] *Shanghai Institute of Ceramics, Chinese Academy of Sciences, 585 Heshuo Road, Shanghai 201800, China. E-mail: xxfshcn@163.com, jingsun@mail.sic.ac.cn*
[b] *University of Chinese Academy of Sciences, 19 Yuquan Road, Beijing 100049, China*
[c] *Guo Neng Yunnan New Power Co., Guangfu Road, Kunming 650299, China*

† Electronic supplementary information (ESI) available. See DOI: https://doi.org/10.1039/d4cp00459k

(TM^{n+}) ion doping can effectively utilize and regulate the luminescence efficiency of Ln^{3+} ions.[22] A variety of TM^{n+} ions (such as Mn^{2+},[23] Fe^{3+},[24] Cu^{2+},[25] Zn^{2+},[26–28] Zr^{4+},[29] and Mo^{2+30}) doped upconversion luminescence materials have been well studied. Chauhan *et al.* prepared Zn^{2+} doped $GdVO_4$:Yb^{3+}/Er^{3+} by using a co-precipitation method, and attempted to independently analyze the effects of lattice shrinkage and particle size on luminescence intensity.[31] Du *et al.* synthesized Cu^{2+} doped $NaYF_4$:Yb/Er microrods *via* a solvothermal method to control the crystal phase and size at the same time, and enhanced the green and red emissions by 37 and 25 times, respectively.[25] However, there are few reports on the study of Co^{2+} ion doped $NaYF_4$:Ln^{3+} systems, especially in the field of photovoltaic efficiency enhancement.

Here, we proposed a new approach to improve the upconversion luminescence intensity of $NaYF_4$:Yb/Er/Tm *via* Co^{2+} ion doping. A series of Co^{2+} ion doped $NaYF_4$:Yb/Er/Tm upconversion luminescent materials were prepared by using a hydrothermal method using rare earth nitrates as precursors. Compared with the undoped sample, the $NaYF_4$:Yb/Er/Tm doped with Co^{2+} had stronger luminescence properties. We systematically studied the luminescence properties under different concentrations of Co^{2+} ion doping and explained the reason for Co^{2+} ion doping enhanced luminescence. Finally, the application potential of the prepared Co^{2+} ion doped $NaYF_4$:Yb/Er/Tm in enhancing the photoelectric conversion efficiency of photovoltaic cells was demonstrated.

2. Results and discussion

2.1. Structure and morphology characterization

The phase composition analysis of the $NaYF_4$:Yb/Er/Tm/Co (18/2/2/*x* mol%, *x* = 0, 5, 15, and 25) samples characterized by XRD (Fig. 1) showed the phase of the β-$NaYF_4$ crystal structure. The diffraction peaks correspond well to JCPDS 28-1192, and the major diffraction peaks located at 17.137°, 29.960°, 30.807°, 43.472°, and 53.716° correspond to the (100), (110), (101), (201), and (211) crystal planes of $NaYF_4$ (Fig. 1a). It is obvious that the diffraction peak intensity decreases with the increase of Co^{2+} ion doping compared with the undoped Co^{2+} ion sample. The decrease of diffraction peak intensity may be caused by structural changes in the crystal. To further investigate the effect of Co^{2+} ions doping on crystal structure, the diffraction peaks located at 29°–32° were amplified. As shown in Fig. 1b, the (110) and (101) diffraction peaks shift to lower angles after Co^{2+} ion doping. According to Bragg's formula, diffraction peaks located at lower angles correspond to larger lattice parameters. This phenomenon may be related to the substitution of impurity ions at the lattice sites or the occupation of interstitial positions. Such results are also observed in Ba^{2+} ions doped $LaVO_4$:Yb^{3+}/Er^{3+} nanorods.[21] The unit cell parameters of as-prepared samples were calculated by using the measured XRD data. As shown in Table 1, it can be observed that the grain size increases with the addition of Co^{2+} ions doping. Consistent with the above analysis results, it is proved that Co^{2+} ions are successfully doped into the crystal.

The microscopic morphologies of the synthesized $NaYF_4$:Yb/Er/Tm/Co (18/2/2/*x* mol%, *x* = 0, 5, 15, and 25) samples were observed by SEM (Fig. 2). The sample of undoped Co^{2+} ions showed the typical hexagonal morphology of the β-$NaYF_4$ crystal (Fig. 2a) with a diameter of 2.778 μm and a side length of 1.411 μm (Fig. S1a, ESI†), while it is relatively thin at 133.3 nm (Fig. S2a, ESI†). When the doped amount of Co^{2+} ions is 5 mol% (Fig. 2b), the particle size decreases to 1.968 μm in diameter, and 967.4 nm in side length (Fig. S1b, ESI†) and increases to about 200 nm in thickness. At the same time, gully stripes can be seen on the surface (Fig. S2b, ESI†). It may be that the doping of Co^{2+} ions affected the crystal growth, and the force generated by surface charge compensation reduced the crystallinity of the crystal and made the surface loose. With the further increase of Co^{2+} ions, the sample size first increased and then decreased, the diameter changed from 4.654 μm to 1.642 μm, the side length changed from 2.260 μm to 846.2 nm (Fig. S1c and d, ESI†), and the thickness changed from 1.213 μm to 693.7 nm (Fig. S2c and d, ESI†). The crystallinity was improved with the hexagonal columnar and smoother morphology due to

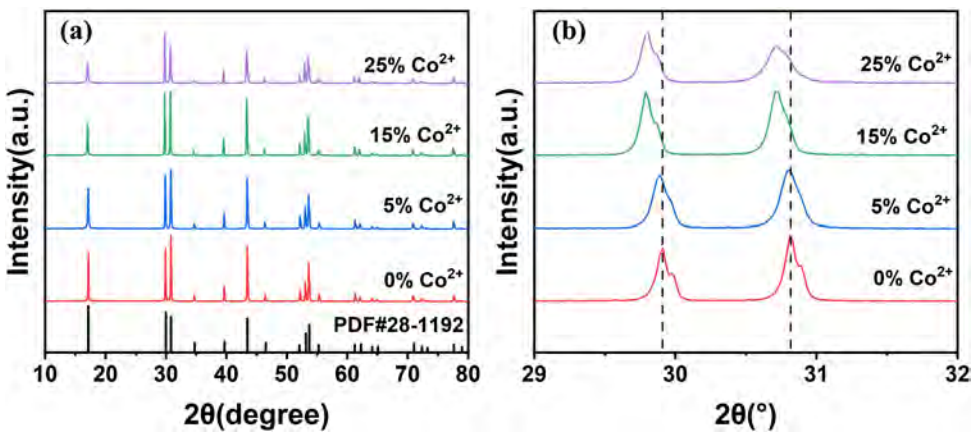

Fig. 1 (a) XRD patterns of $NaYF_4$:Yb/Er/Tm/Co (18/2/2/*x* mol%, *x* = 0, 5, 15, 25) samples; (b) magnified XRD patterns of diffraction peaks range from 29 to 32 degrees.

Table 1 Cell parameters of as-prepared $NaYF_4$:Yb/Er/Tm/Co (18/2/2/*x* mol%, *x* = 0, 5, 15, 25) samples

No.	Co^{2+} doping content *x* (%)	Lattice parameter (Å)		Cell volume (Å^3)
		a	*c*	
1	0	5.96	3.51	107.98
2	5	5.97	3.55	126.52
3	15	5.99	3.56	127.73
4	25	5.98	3.56	127.31

reduced surface defects. The size evolution of $NaYF_4$ may be due to the effect of Co^{2+} dopant ions on the crystal growth through surface charge modification, since the Co^{2+} ions differ in their valence states from the Y^{3+} or F^- ions that may be substituted.[32]

We further investigated the structure and element distribution of the $NaYF_4$:Yb/Er/Tm microcrystals with 5 mol% Co^{2+} ion doping (Fig. 3). As shown in Fig. 3a, the microcrystal appears to have a hexagonal structure of uniform growth. The high-resolution TEM image suggested the distinct lattice fringes in $NaYF_4$:Yb/Er/Tm microcrystals with 5 mol% Co^{2+} ion doping with a lattice spacing of 0.511 nm, which was attributed to the (100) crystal plane of the β-$NaYF_4$ crystal (Fig. 3b). The (101) and (110) crystal planes of the β-$NaYF_4$ crystal were further marked by selected area electron diffraction (SAED) pattern taken at [001] incidence.[32] The peaks of Na, Y, F, Yb, Er, Tm and Co elements can be clearly observed from the EDS spectra in Fig. 3c, which proved that the Co^{2+} ions and lanthanide elements (Yb^{3+}, Er^{3+}, and Tm^{3+}) were successfully doped in the lattice of the β-$NaYF_4$ crystal.[33] The high content of Co^{2+} ions and the low content of Er^{3+} may be due to the error caused by the coincidence of their main peak positions at about 7 keV. At the same time, the element mapping results show that each element was uniformly distributed in the $NaYF_4$:Yb/Er/Tm microcrystals with 5 mol% Co^{2+} ion doping.

As shown in Fig. 4, the surface chemical composition and valence state of the elements in the $NaYF_4$:Yb/Er/Tm/Co (5 mol% Co^{2+} ions doping) were characterized by X-ray photoelectron spectroscopy (XPS).[34] The XPS survey spectrum reveals the presence of Na, Y, F, Yb, Er, Tm and Co elements (Fig. 4a).[25] The peaks located at 1071.93 eV and 685.23 eV could be attributed to Na 1s and F 1s (Fig. 4b and d), respectively. The peaks located at 159.24 eV and 161.28 eV can be assigned to Y $3d_{5/2}$ and $3d_{3/2}$ (Fig. 4c), respectively. The peaks located at 172.18 eV, 174.60 eV and 186.70 eV could be attributed to Er 4d, Tm 4d and Yb 4d (Fig. 4e), respectively. The peaks located at 780.22 eV and 794.76 eV correspond to Co $2p_{3/2}$ and Co $2p_{1/2}$ (Fig. 4f), respectively.[35] In addition, the peaks located at 782.99 eV and 800.18 eV could be attributed to the companion satellite peaks of Co.[36] We analyzed the XPS spectra of Co 2p, Na 1s, Y 3d, and F 1s of four $NaYF_4$:Yb/Er/Tm/Co (18/2/2/*x* mol%, *x* = 0, 5, 15, and 25) samples (Fig. S3, ESI†). With the increase of Co^{2+} ion doping, the binding energy of Co 2p increases gradually, but the binding energy of other elements is almost unchanged. We hypothesize that Co^{2+} ions occupy interstitial positions in the lattice, rather than displacing other atoms, thus causing the lattice to expand.[20] The XPS measured actual molar ratios of prepared $NaYF_4$:Yb/Er/Tm/Co (18/2/2/*x* mol%, *x* = 0, 5, 15, and 25) samples are shown in Table S1 (ESI†). It can be seen from Table S1 (ESI†) that with the decrease of Y^{3+} ions, the Co^{2+} ions in the sample gradually increase, which once again proves that Co^{2+} ions were successfully doped into the $NaYF_4$:Yb/Er/Tm crystal.

Ultraviolet-visible-near infrared (UV-Vis-NIR) absorption spectra (Fig. 5a) reveals that $NaYF_4$:Yb/Er/Tm/Co (18/2/2/*x* mol%, *x* = 0, 5, 15, and 25) samples have an obvious absorption peak at 980 nm, which is related to the electron transition $^2F_{7/2} \rightarrow {}^2F_{5/2}$ of Yb^{3+} ions absorbing photons.[37] The chemical structures of $NaYF_4$:Yb/Er/Tm/Co (18/2/2/*x* mol%, *x* = 0, 5, 15, and 25) samples were detected by infrared spectroscopy (IR) in Fig. 5b. The peaks in around 1500 cm^{-1} to 1630 cm^{-1} originate from the stretching vibrations of –COO^-, and the absorption

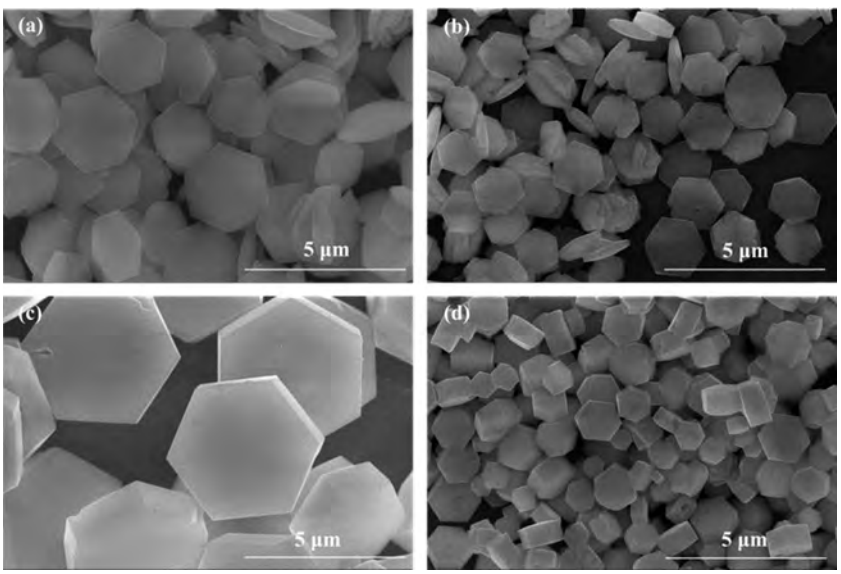

Fig. 2 SEM images of $NaYF_4$:Yb/Er/Tm/Co (18/2/2/*x* mol%, *x* = 0, 5, 15, 25) samples: (a) *x* = 0, (b) *x* = 5, (c) *x* = 15 and (d) *x* = 25.

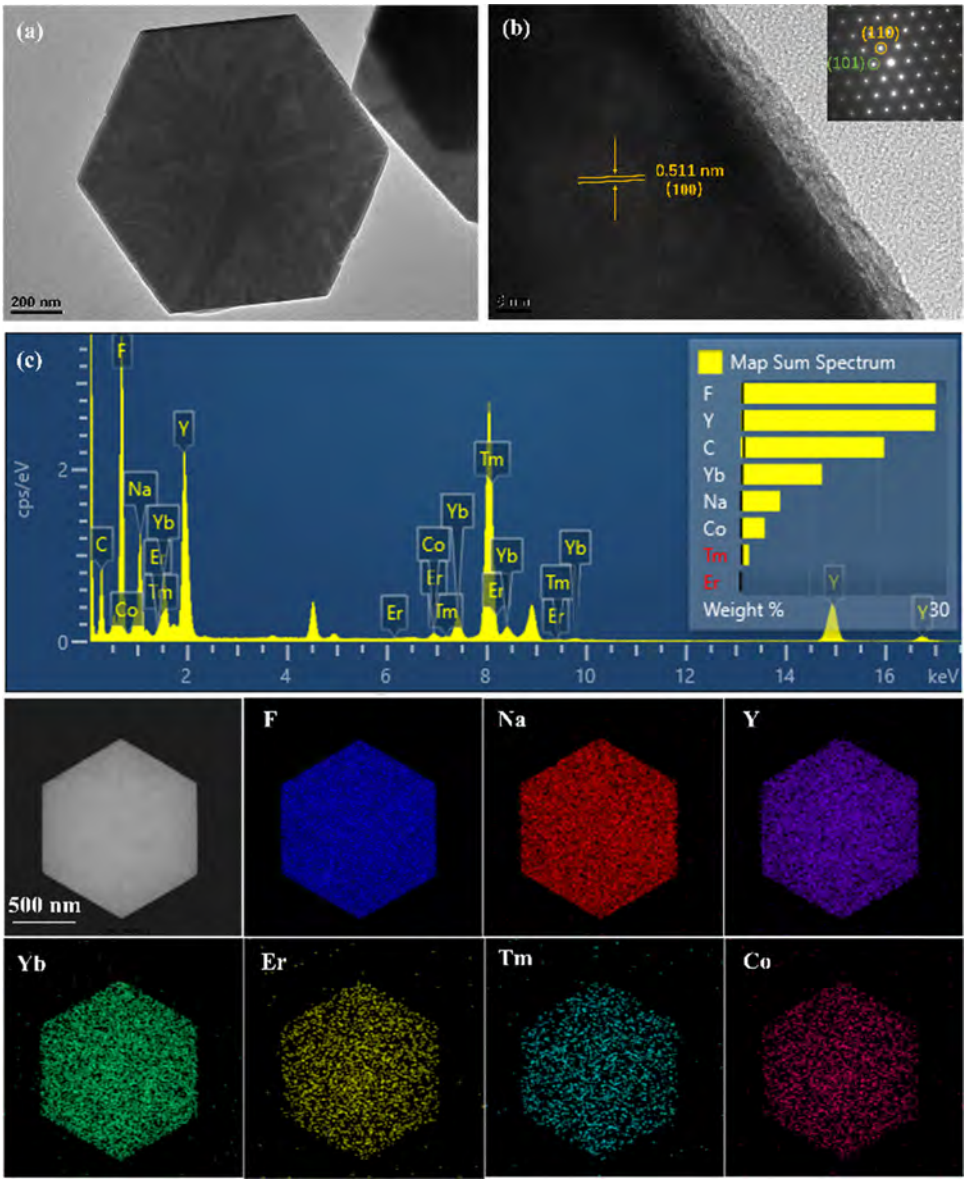

Fig. 3 (a) TEM image, (b) high-resolution TEM image and Selected area electron diffraction (SAED) pattern taken in [001] incidence (top right corner), (c) EDS spectra and element mapping images of $NaYF_4$:Yb/Er/Tm crystals doped with 5 mol% Co^{2+} ions.

peak near 3470 cm^{-1} is due to the stretching vibration of the –OH group.[38] The peaks near 2300 cm^{-1} to 2400 cm^{-1} may originated from the formation of hydrogen bonds between –COOH and the linker, resulting in a weak hydroxyl vibration peak.

2.2. Upconversion luminescence properties and mechanism

Fig. 6 shows the upconversion luminescence spectra of $NaYF_4$: Yb/Er/Tm crystals doped with Co^{2+} ions at different concentrations, which were excited by a 980 nm laser. As shown in Fig. 6a, the upconversion emission peak at 487 nm is originated from the $^1G_4 \rightarrow {}^3H_6$ transition of Tm^{3+} ions.[39] The upconversion emission peak at 521 nm, 540 nm, 654 nm are originated from the $^2H_{11/2} \rightarrow {}^4I_{15/2}$, $^4S_{3/2} \rightarrow {}^4I_{15/2}$, $^4F_{9/2} \rightarrow {}^4I_{15/2}$ transition of Er^{3+} ions, respectively.[40] The energy transfer process and upconversion luminescence mechanism of $NaYF_4$:Yb/Er/Tm crystals is shown in Fig. 7. The relationship between green and red luminescence intensity and Co^{2+} ions doping amount can be seen in Fig. 6b. When the doping amount of Co^{2+} ions is 5 mol%, there is the highest emission intensity of green and red luminescence. Compared with the sample of undoped Co^{2+} ions, the green and red luminescence intensity were enhanced 18.19% and 83.24%, respectively. The results of luminescence lifetime decay (Fig. 6c and d) are consistent with the results of luminescence intensity.[41] The highest luminescence lifetime is obtained when the doping amount of Co^{2+} ions is 5 mol%, which again proves that the optimal doping amount of Co^{2+} ions is about 5 mol%.

To further explore the influence of Co^{2+} ions doping on the luminescence process, the logarithmic curve of luminescence intensity and excitation power is plotted in Fig. 8a and 8b. The

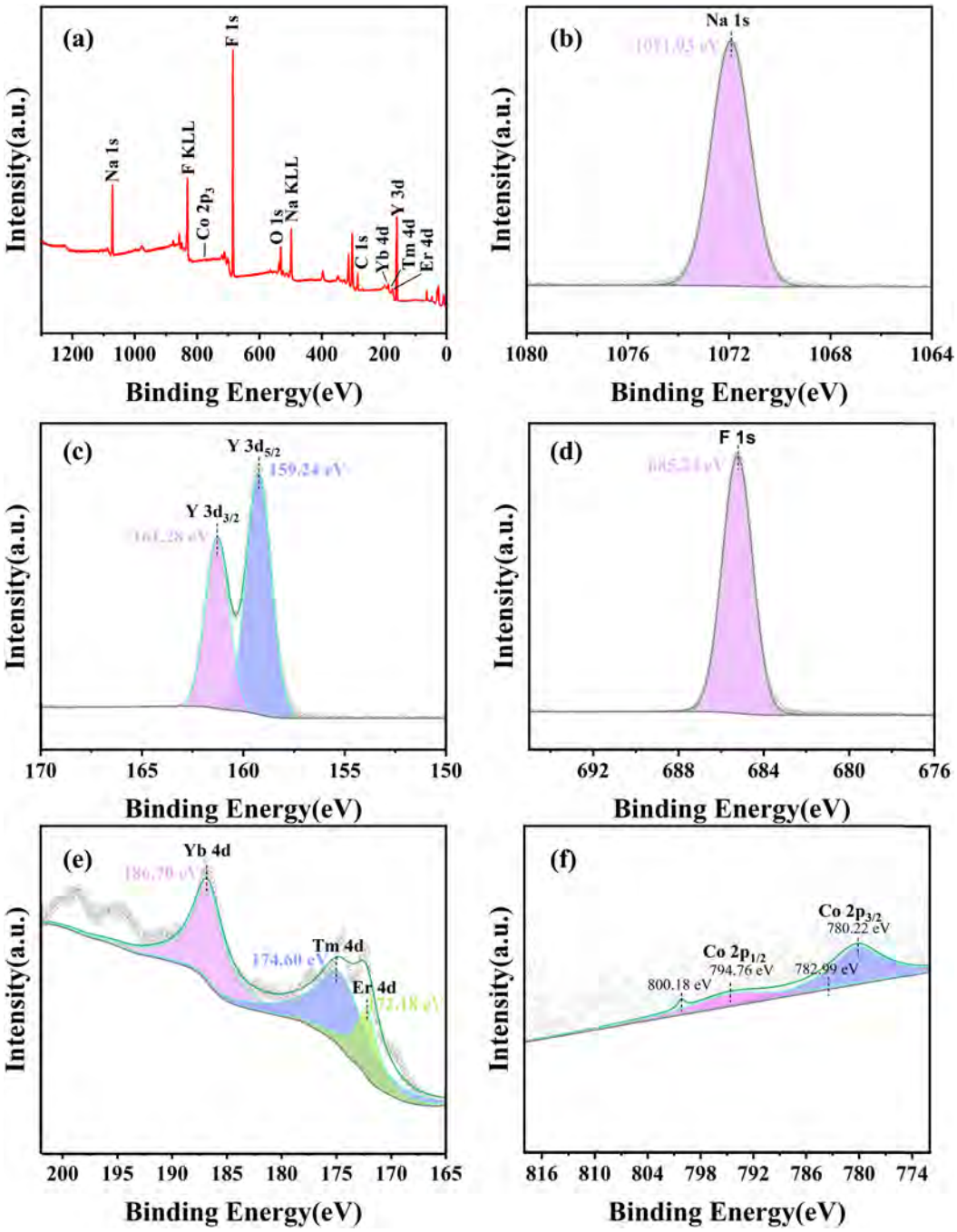

Fig. 4 XPS (a) survey, (b) Na 1s, (c) Y 3d, (d) F 1s, (e) Yb, Er and Tm 4d, (f) Co 2p spectra of $NaYF_4$:Yb/Er/Tm crystals doped with 5 mol% Co^{2+} ions.

relationship between luminescence intensity and excitation power can be described by the following formula:

$$I_{UC} \propto P^n \quad (1)$$

where I_{UC} is the luminescence intensity, P is excitation power and n is the number of photons required for certain emission states.[42] By fitting the curves, it is calculated that the slope of the curves with the emission peak at 520 nm, 540 nm and 654 nm are close to 2, indicating that the upconversion luminescence is a two-photon process. The addition of Co^{2+} ions did not change the two-photon process. To investigate the effect of Co^{2+} ions doping on the crystal field symmetry of activator ions Er^{3+} and Tm^{3+} in the $NaYF_4$ crystal, Eu^{3+} was used as a structural probe to analyze the change (Fig. 8c).[43] Since the $^5D_0 \rightarrow {}^7F_1$ transition does not depend on the ligand field and $^5D_0 \rightarrow {}^7F_2$ transition increases with decreasing environmental symmetry, the $^5D_0 \rightarrow {}^7F_1/{}^5D_0 \rightarrow {}^7F_2$ intensity ratio is used to characterize the crystal field symmetry of activator ions in the crystal (Fig. 8d). The $^5D_0 \rightarrow {}^7F_1/{}^5D_0 \rightarrow {}^7F_2$ intensity ratio increases with the increase of Co^{2+} ions doping but decreases

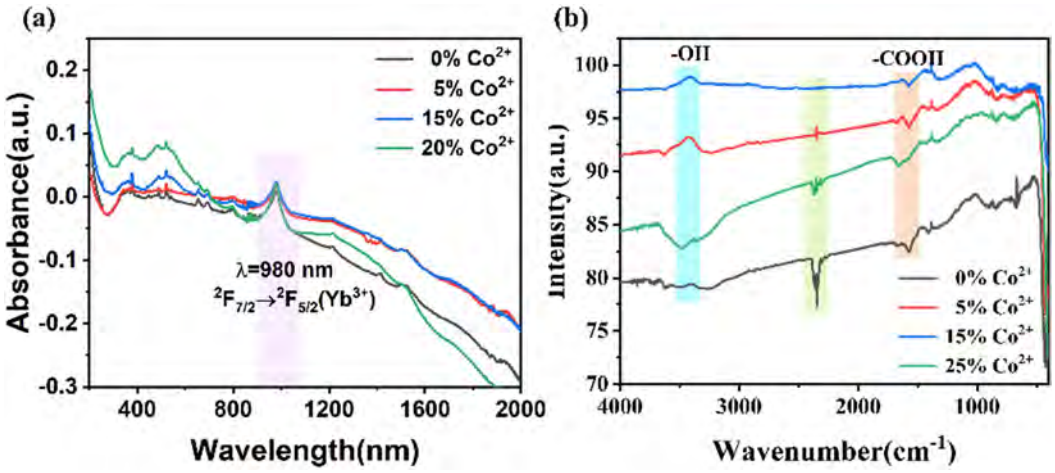

Fig. 5 (a) UV-Vis-IR diffuse reflectance spectra and (b) IR spectra of $NaYF_4$:Yb/Er/Tm/Co (18/2/2/*x* mol%, *x* = 0, 5, 15, and 25) samples.

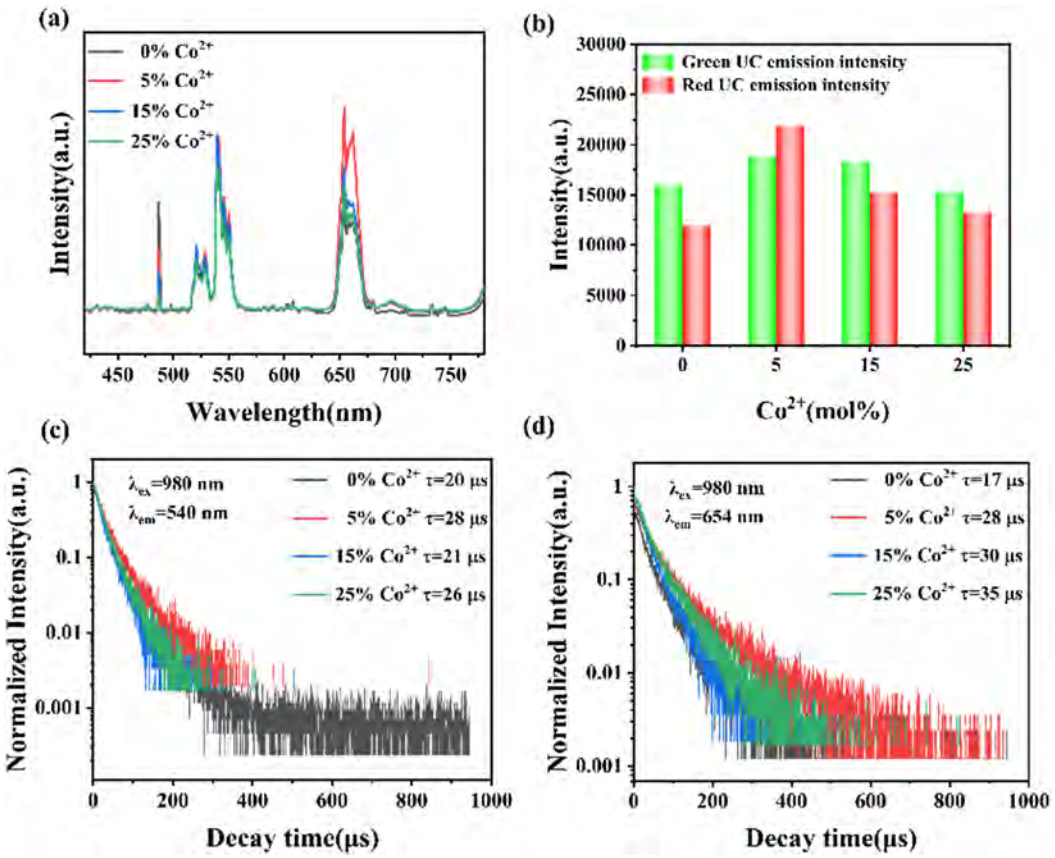

Fig. 6 (a) Upconversion emission spectra of $NaYF_4$:Yb/Er/Tm/Co (18/2/2/*x* mol%, *x* = 0, 5, 15, and 25) samples under a 980 nm laser excitation; (b) the green and red upconversion emission intensity *versus* Co^{2+} ions doping concentration. Upconversion emission fluorescence lifetime spectra of $NaYF_4$:Yb/Er/Tm/Co (18/2/2/*x* mol%, *x* = 0, 5, 15, and 25) samples under a 980 nm laser excitation: (c) Er^{3+}: $^4S_{3/2} \rightarrow {}^4I_{15/2}$ and (d) $^4F_{9/2} \rightarrow {}^4I_{15/2}$ transitions.

when the Co^{2+} ions doping reaches 25 mol%. This shows that the crystal field symmetry of activator ions decreases with the addition of a certain amount of Co^{2+} ions, while the crystal field symmetry of activator ions increases again with the addition of too much Co^{2+} ions due to the increase of crystal crystallinity. The decrease in the local crystal field symmetry of the activator ions breaks the forbidden transition rule, which is conducive to the transition of the f–f electronic state and enhances the upconversion luminescence.[24] This result in Fig. 8d confirms the influence of Co^{2+} ion doping amount on the luminescence intensity.

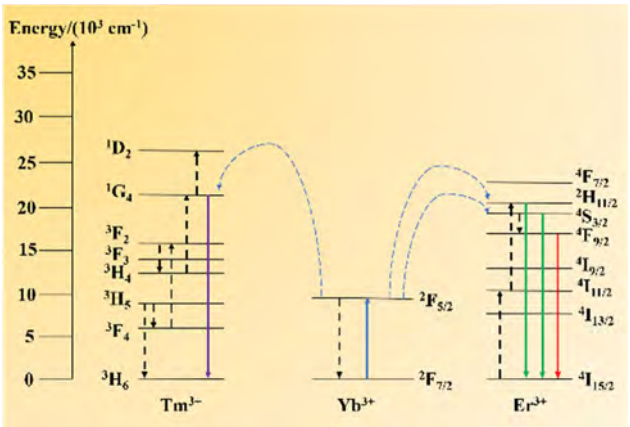

Fig. 7 Energy transfer process and upconversion luminescence mechanism of $NaYF_4$:Yb/Er/Tm crystals.

2.3. Efficiency enhancement of PV cells

The tests of the *J–V* curves were carried out in the solar simulator as shown in Fig. S4 (ESI†). First, the positive and negative electrodes of the photovoltaic cell were connected to the solar simulator (Fig. S4a, ESI†), and then the glass sheet coated with samples was placed on the photovoltaic cell for photoelectric conversion test (Fig. S4b, ESI†). The photoelectric conversion parameters of the cell under infrared (IR) irradiation (Fig. S4c, ESI†) were also tested under the conditions of the filter (photon wavelength $\geq$ 760 nm).

The light transmittance of the glass substrate before and after coating the $NaYF_4$:Yb/Er/Tm/Co (18/2/2/*x* mol%, *x* = 0, 5, 15, and 25) samples was tested (Table 2). The glass substrate before and after coating has basically no decrease in the visible light transmittance. *J–V* curves tested both under one standard solar intensity irradiation (AM1.5G, 100 mW cm^{-2}) and under IR ($\geq$760 nm) radiation are shown in Fig. 9. In addition, the partial magnification curves of Fig. 9a and Fig. 9c are shown in Fig. 9b and Fig. 9d, respectively. The short circuit current density of the samples coated under solar radiation slightly decreases compared with blank glass but increases under IR light. Electrical parameters of the photovoltaic cell covered with different samples under standard solar irradiation (AM1.5G, 100 mW cm^{-2}) and IR light are shown in Table 3 and Table 4. When the photovoltaic cell is covered only by glass without coating, the photoelectric conversion efficiency (E_{ff}) obtained by tested was 12.97% (Table 3). However, after coating the $NaYF_4$:Yb/Er/Tm/Co (18/2/2/*x* mol%, *x* = 0, 5, 15, 25) samples, the efficiency increased to different degrees. According to the

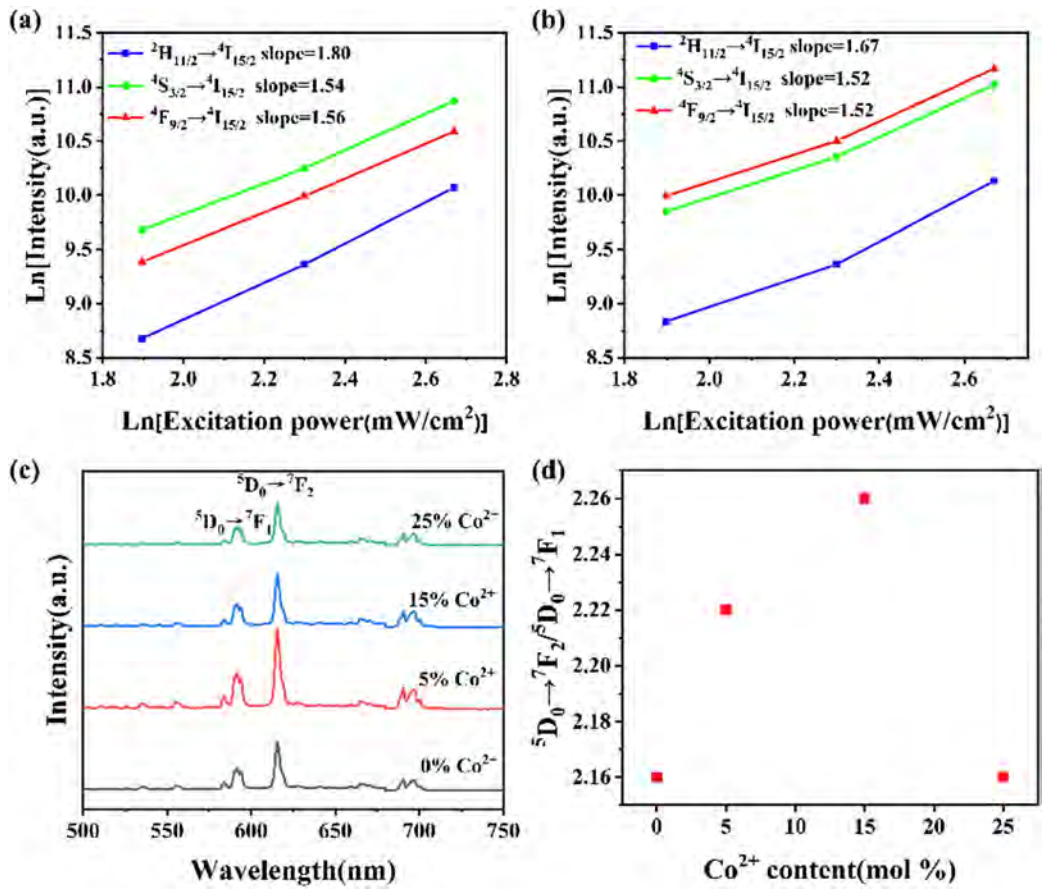

Fig. 8 Upconversion emission peak intensity *versus* laser excitation power of $NaYF_4$:Yb/Er/Tm samples: (a) without and (b) with 5% Co^{2+} ion doping. (c) Emission spectra of $NaYF_4$:Yb/Eu/Co (18/2/*x* mol%, *x* = 0, 5, 15, 25) samples under a 395 nm laser excitation; (d) dependence of $^5D_0 \rightarrow {}^7F_2/{}^5D_0 \rightarrow {}^7F_1$ emission intensity ratio on Co^{2+} doping content.

Table 2 Transmittance of glass substrates coated with the samples

Sample	380–760 nm Tave (%)		760–2500 nm Tave (%)		200–380 nm Tave (%)	
	Blank glass	Glass with coating	Blank glass	Glass with coating	Blank glass	Glass with coating
0% Co^{2+}	96	96	83.2	83.2	91	91
5% Co^{2+}	96	96	83.1	83.5	91	91
15% Co^{2+}	96	96	83.1	82.3	91	91
25% Co^{2+}	96	96	83.2	82.3	91	91

Table 3 Electrical parameters of the photovoltaic cell covered with different samples under one standard solar intensity irradiation (AM1.5G, 100 mW cm^{-2})

Sample	J_{sc} (mA cm^{-2})	V_{oc} (V)	FF (%)	E_{ff} (%)	Overall increase (%)
Blank glass	7.50	2.40	71.98	12.97	—
0% Co^{2+}	7.48	2.43	72.36	13.16	1.46
5% Co^{2+}	7.48	2.44	72.45	13.24	2.08
15% Co^{2+}	7.47	2.46	72.50	13.21	1.85
25% Co^{2+}	7.46	2.44	72.57	13.22	1.93

Table 4 Electrical parameters of the photovoltaic cell covered with different samples under IR light (>760 nm)

Sample	J_{sc} (mA cm^{-2})	V_{oc} (V)	FF (%)	E_{ff} (%)	Overall increase (%)
Blank glass	2.90	2.30	74.62	4.98	—
0% Co^{2+}	2.91	2.33	74.84	5.06	1.61
5% Co^{2+}	2.90	2.33	75.04	5.08	2.01
15% Co^{2+}	2.89	2.34	75.05	5.06	1.61
25% Co^{2+}	2.91	2.33	74.99	5.09	2.21

calculations, the relative value of the increase in the efficiency of the samples from 0 mol% to 25 mol% Co^{2+} ions doping is 1.46%, 2.08%, 1.85% and 1.93%, respectively. Therefore, when the Co^{2+} ion doping amount is 5 mol%, the efficiency of the photovoltaic cell increases the most under solar irradiation, which is consistent with the results of the above luminescence intensity (Fig. 6a). Compared with previous studies (Table S2, ESI†), 5% Co^{2+} ion doped $NaYF_4$:Yb/Er/Tm upconversion luminescence material still exhibited advantages of the efficiency enhancement of the photovoltaic cell. The initial efficiency of the blank glass covered photovoltaic cell under IR irradiation is 4.98% (Table 4). The relative value of the increase in the efficiency of the samples from 0 mol% to 25 mol% Co^{2+} ion doping is 1.61%, 2.01%, 1.61% and 2.21%, respectively. To make the data more intuitive, we plotted the enhanced values of efficiency of the photovoltaic cell in Table 3 and Table 4 in a bar chart (Fig. S5, ESI†). The results show that the prepared

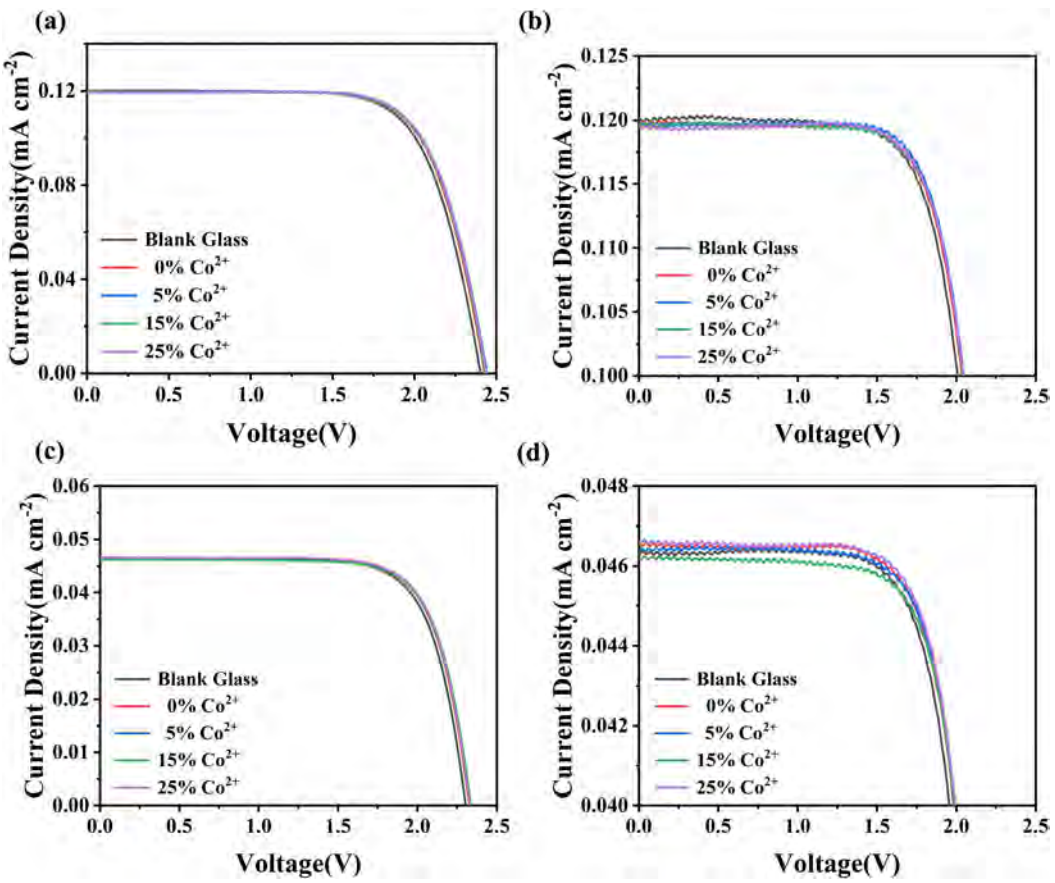

Fig. 9 (a) *J*–*V* curve tested under one standard solar intensity irradiation (AM1.5G, 100 mW cm^{-2}) and (b) a partial magnification of (a); (c) *J*–*V* curve tested under IR light (a filter was used to remove ultraviolet and visible light from solar irradiation, photon wavelength ≥ 760 nm) and (d) a partial magnification of (c).

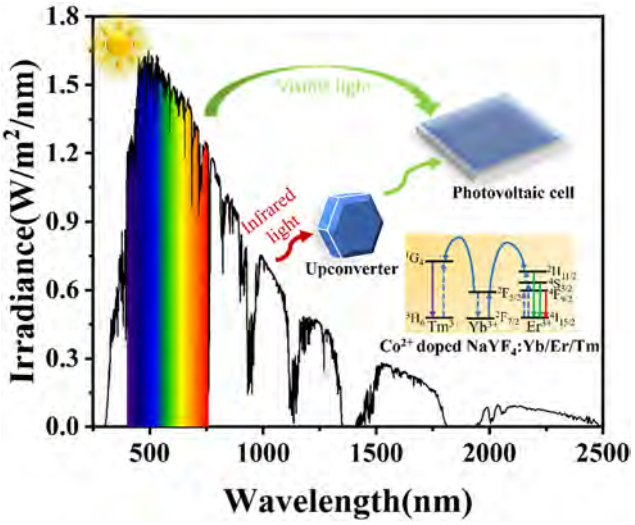

Fig. 10 Proposed mechanism for the efficiency enhancement of the photovoltaic cell over the Co^{2+} ion doped $NaYF_4$:Yb/Er/Tm upconversion luminescence microcrystal.

$NaYF_4$:Yb/Er/Tm upconversion luminescence materials with Co^{2+} ion doping can absorb IR photons and convert them into visible photons used by photovoltaic cells, and broaden the utilization range of sunlight by photovoltaic cells.

The proposed mechanism diagram for the efficiency enhancement of photovoltaic cell over the Co^{2+} ion doped $NaYF_4$:Yb/Er/Tm upconversion luminescence microcrystal is shown in Fig. 10. Transition metal Co^{2+} ions doped $NaYF_4$:Yb/Er/Tm upconversion luminescent microcrystal was successfully prepared and as coating employed for improving the efficiency of photovoltaic cells. It's speculated that Co^{2+} ion doped $NaYF_4$:Yb/Er/Tm microcrystal improved the crystallinity and reduced the crystal field symmetry of activator ions (Er^{3+} and Tm^{3+}) in the upconversion luminescent material system, thus contributing to the electron transition in the 4f–4f configuration.[44] Therefore, the efficiency of energy transfer and conversion was improved.[45] The improved efficiency of photovoltaic cell indicates that Co^{2+} doped $NaYF_4$:Yb/Er/Tm microcrystal could make full use of infrared photons to convert visible photons required by photovoltaic cells.

3. Conclusion

In summary, a novel approach was proposed to improve the efficiency of the photovoltaic cell with the Co^{2+} doped $NaYF_4$:Yb/Er/Tm upconversion luminescent material. Different ratios of Co^{2+} modulated the morphology and crystallinity of upconversion luminescent $NaYF_4$:Yb/Er/Tm microcrystals, with the best Co-doped $NaYF_4$:Yb/Er/Tm coating sample showing excellent upconversion luminescence intensity and fluorescence lifetime. The emission intensity of green and red light was enhanced by 18.19% and 83.24%, respectively. Experiments revealed that the crystal field symmetry of activator ions decreased after Co^{2+} doping. The photoelectric efficiency of $NaYF_4$:Yb/Er/Tm coating with 5% Co^{2+} doping on the surface of photovoltaic cell was increased by 2.08% and 2.01% under solar and infrared (≥760 nm) irradiation, respectively. The reason is that the energy transfer and conversion efficiencies have been improved, and $NaYF_4$:Yb/Er/Tm/Co microcrystals can make more use of the light energy in the infrared band. This work provides a new path to increase the utilization of infrared light in the solar spectrum and improve the photoelectric conversion efficiency of photovoltaic cells.

Conflicts of interest

The authors declare no conflict of interest.

Acknowledgements

This work was financially supported by the Project of CHN Energy Investment Group (XNYGS-2023-422) and Inner Mongolia Key R&D Plan (2022YFHH0049).

References

1 P. Zhang, L. Liang and X. Liu, *J. Mater. Chem. C*, 2021, **9**, 16110–16131.
2 J. Jin, Q. Cao, L. Zhao, Y. Zhou, Z. Li, L. Gui, Z. Chen, C. Wu, S. Wang and B. Chi, *Mater. Today Commun.*, 2022, **33**, 104513–104521.
3 F. L. Meng, J. J. Wu, E. F. Zhao, Y. Z. Zheng, M. L. Huang, L. M. Dai, X. Tao and J. F. Chen, *Nanoscale*, 2017, **9**, 18535–18545.
4 J. C. Goldschmidt and S. Fischer, *Adv. Opt. Mater.*, 2015, **3**, 510–535.
5 X. Huang, S. Han, W. Huang and X. Liu, *Chem. Soc. Rev.*, 2013, **42**, 173–201.
6 C. Chen, C. Li and Z. Shi, *Adv. Sci.*, 2016, **3**, 1600029.
7 J. Zhou, Q. Liu, W. Feng, Y. Sun and F. Li, *Chem. Rev.*, 2015, **115**, 395–465.
8 L. Wang, P. Li and Y. Li, *Adv. Mater.*, 2007, **19**, 3304–3307.
9 L. Wang, X. Li, Z. Li, W. Chu, R. Li, K. Lin, H. Qian, Y. Wang, C. Wu, J. Li, D. Tu, Q. Zhang, L. Song, J. Jiang, X. Chen, Y. Luo, Y. Xie and Y. Xiong, *Adv. Mater.*, 2015, **27**, 5528–5533.
10 H. Ji, J. Tang, X. Tang, Z. Yang, H. Zhang and Y. Qian, *Mater. Lett.*, 2021, **302**, 130348–130351.
11 S. Som, C.-Y. Yang, C.-H. Lu and S. Das, *Ceram. Int.*, 2019, **45**, 5703–5709.
12 Z. Lei, X. Ling, Q. Mei, S. Fu, J. Zhang and Y. Zhang, *Adv. Mater.*, 2020, **32**, e1906225.
13 C. Homann, L. Krukewitt, F. Frenzel, B. Grauel, C. Wurth, U. Resch-Genger and M. Haase, *Angew. Chem., Int. Ed.*, 2018, 57, 8765–8769.
14 J. Hu, X. Bian, R. Wang, L. Liu, N. Ilyas, F. Wang, Z. Song and H. Fu, *Chem. Mater.*, 2022, **34**, 3089–3098.
15 W. Gao, Z. Sun, Q. Han, S. Han, X. Cheng, Y. Wang, X. Yan and J. Dong, *J. Alloys Compd.*, 2021, **857**, 157578–157588.

16 H. Zhou, J. Zou, X. Weng, Y. Lai and J. Yu, *Opt. Mater*, 2023, **137**, 113590–113595.
17 J. Chen, X. Lu, Y. Chen, J. Shuai, J. Gao, X. Liu and W. Feng, *Mater. Lett.*, 2023, **352**, 135121–135124.
18 H. Fu, C. Hu, J. Liu, Q. Zhang, J. Y. Xu, G. J. Jiang and M. Liu, *CrystEngComm*, 2022, **24**, 7698–7717.
19 X. Jin, S. W. Leow, Y. Fang and L. H. Wong, *J. Mater. Chem. A*, 2023, **11**, 12992–12998.
20 D. Chen and Y. Wang, *Nanoscale*, 2013, **5**, 4621–4637.
21 M. Chen, L. Zeng, H. Zhou, J. Zeng, X. Wang, T. Pang, J. Tang and D. Chen, *Ceram. Int.*, 2023, **49**, 32000–32007.
22 S. Mohanty and A. M. Kaczmarek, *Chem. Soc. Rev.*, 2022, **51**, 6893–6908.
23 Y. H. Kim, J. Ha and W. B. Im, *J. Mater. Res. Technol.*, 2021, **11**, 181–195.
24 J. Tang, L. Chen, J. Li, Z. Wang, J. Zhang, L. Zhang, Y. Luo and X. Wang, *Nanoscale*, 2015, **7**, 14752–14759.
25 K. Du, X. Xu, S. Yao, P. Lei, L. Dong, M. Zhang, J. Feng and H. Zhang, *CrystEngComm*, 2018, **20**, 1945–1953.
26 T. Cong, Y. Ding, J. Liu, H. Zhao and X. Hong, *Mater. Lett.*, 2016, **165**, 59–62.
27 Y. Wang, Z. Wen, W. Ye, Z. Feng, C. Zhao, C. Zuo, Y. Li, Z. Cao, Z. Cao, C. Ma and Y. Cao, *J. Lumin.*, 2020, **221**, 117029–117035.
28 M. Sun, J. Liu and L. Nie, *J. Alloys Compd.*, 2020, **816**, 152575–152582.
29 S. Namagal, N. Victor Jaya, N. Nithyaa, M. Muralidharan and S. Venkatesh, *J. Inorg. Organomet. Polym. Mater.*, 2022, **32**, 3128–3140.
30 D. Yin, C. Wang, J. Ouyang, K. Song, B. Liu, X. Cao, L. Zhang, Y. Han, X. Long and M. Wu, *Dalton Trans.*, 2014, **43**, 12037–12043.
31 A. Chauhan, S. Kataria, D. Busko, F. A. Cardona, A. Turshatov and B. S. Richards, *J. Mater. Chem. C*, 2021, **9**, 16709–16720.
32 F. Wang, Y. Han, C. S. Lim, Y. Lu, J. Wang, J. Xu, H. Chen, C. Zhang, M. Hong and X. Liu, *Nature*, 2010, **463**, 1061–1065.
33 Z. Zhang, X. Yu, X. Xue, B. Gao, Y. Bai, H. Yang, X. Li, J. Fan and P. Zhao, *J. Alloys Compd.*, 2023, **930**, 167357–167366.
34 C. Jia, B. Wan, W. Liu, L. Qi, X. Liu, X. Han, A. Gao and J. Liu, *Adv. Funct. Mater.*, 2023, **34**, 2311663–2311673.
35 Q. Zhang, P. Yang, H. Zhang, J. Zhao, H. Shi, Y. Huang and H. Yang, *Appl. Catal., B*, 2022, **300**, 120729–120740.
36 Y. Xie, Y. Wang, Y. Zhou, F. Wang, Y. Xu, S. Rao and J. Zhao, *Appl. Catal., A*, 2024, **669**, 119504–119512.
37 A. Jarosz-Duda, P. O'Callaghan, J. Kuncewicz, P. Łabuz and W. Macyk, *Catalysts*, 2020, **10**, 232–241.
38 H. Tang, Y. Xu and X. Cheng, *J. Solid State Chem.*, 2020, **285**, 121229–121236.
39 M. Meng, R. Zhang, X. Fa, J. Yang, Z. Cheng, A. A. Ansari, J. Ou, C. Wurth and U. Resch-Genger, *CrystEngComm*, 2022, **24**, 1752–1763.
40 X. Zhai, Y. Li, W. Zhao, W. Sun, M. He and J. Feng, *J. Rare Earths*, 2023, **41**, 498–506.
41 W. Gao, S. Han, B. Wang, Z. Sun, Y. Lu, Q. Han, X. Yan, J. Liu and J. Dong, *J. Alloys Compd.*, 2022, **900**, 163493–163514.
42 J. Ma, Y. Wei, T. Liu, L. Xu, T. Wang, Z. Song, J. Qiu and Y. Li, *J. Lumin.*, 2023, **260**, 119860–119866.
43 L. Lei, D. Chen, J. Xu, R. Zhang and Y. Wang, *Chem. – Asian J.*, 2014, **9**, 728–733.
44 Y. Wei, P. Dang, Z. Dai, G. Li and J. Lin, *Chem. Mater.*, 2021, **33**, 5496–5526.
45 S. Ye, E. H. Song and Q. Y. Zhang, *Adv. Sci.*, 2016, **3**, 1600302.